RSC Advances

PAPER

View Article Online
View Journal | View Issue

Cite this: *RSC Adv.*, 2016, **6**, 58354

Hexavalent chromium induced tunable surface functionalization of graphite†

Bo Xiang,*[a] Dong Ling,[a] Feng Gao,[a] Han Lou,[a] Hongbo Gu*[a] and Zhanhu Guo*[b]

Received 16th April 2016
Accepted 6th June 2016

DOI: 10.1039/c6ra09847a

www.rsc.org/advances

Hexavalent chromium (Cr(VI)) was chosen to serve as an oxidant to functionalize the surface of graphite. The effect of pH and concentration of Cr(VI) solution on the functionalization of graphite was systematically investigated by Raman spectroscopy, Fourier transform infrared spectroscopy (FT-IR), thermogravimetric analysis (TGA), and X-ray photoelectron spectroscopy (XPS). The results showed that the ether (C–O–C) functional groups were observed on the surface of graphite after being treated with pH = 1.0 solution with a Cr(VI) concentration of 1000 μg L^{-1} for 30 min. However, no obvious functional groups were observed on the graphite surface for the pH higher than 2.0 and the Cr(VI) concentrations higher than 2.0 mg L^{-1}. The electrical conductivity of functionalized graphite by Cr(VI) was observed to be good, *i.e.*, the same order of magnitude as that of the as-received graphite without a serious decrease. This work provides a new strategy to functionalize graphite for preparing multifunctional graphite nanocomposites.

1. Introduction

Graphite, one of the most important and widely used materials, has been applied in the fields of lubricants,[1,2] lithium-ion batteries,[3] piezoresistive sensors,[4] and supercapacitors[5–8] due to its unique properties, including low friction,[9] thermal stability,[10] and electrical conductivity.[7] In graphite, sp^2-hybridized carbons are covalently bonded in a hexagonal manner, forming individual graphene sheets. These sheets are bound together by van der Waals forces,[11] which make it a good material for preparing nanocomposites with excellent thermal, mechanical, and electrical properties.[12] Normally, graphite can be used for reinforcing metal matrix composites. For example, in copper matrix–graphite composites, the thermal conductivity along the alignment direction is up to five times higher than perpendicular direction, whereas the thermal diffusivity is 20% lower compared to copper.[13] It has also been proved that the copper matrix composites could achieve a higher thermal conductivity for transmitting heat and stress than copper by adding graphite platelets.[13,14] The aluminum alloys also showed higher tensile strength, hardness and significantly improved wear resistance compared to the base alloy after adding granite dusts with graphite.[15] In lithium-ion batteries, the Sn–SnO_2/graphite nanocomposites, which was obtained by the chemical reduction and oxidation of Sn nanocrystals onto graphite, showed very stable cyclic performance because the graphite could prevent agglomeration or size growth of nanocrystals and supply electrical conduction.[16] Expandable graphite had been served as an intumescent flame retardant in polyisocyanurate–polyurethane foams and high-density rigid polyurethane foams with an overall improved fire behavior without damaging the mechanical properties of polymer matrix.[17] Graphite nanoplatelets decorated polyurethane nanofiber composites fabricated by the combination of electrospinning and sonication have displayed enhanced thermal stability and hardness originated from the uniform dispersion of graphite nanoplatelets as well as strong interaction between the graphite-nanoplatelet and the nanofibers, in which the electrical conductivity was significantly improved.[18]

However, untreated graphite has few functional groups on the surface, significantly limiting its applications in nanocomposites and biological analytes or enzymes.[19] Introducing functional groups on the surface of graphite can remarkably improve its dispersibility in various organic solvents and matrix,[20,21] and change its conductivity and flexibility for the usage in the flexible electronics.[22] Different functional groups can provide graphite with different properties. For instance, graphite functionalized with L-phenylalanine amino acid onto its edge through direct Friedel–Crafts acylation reaction in polyphosphoric acid/phosphorus pentoxide medium could enhance the electron transfer capability compared to the pristine graphite without damaging the graphitic basal plane and the high crystalline graphitic structure.[23] After functionalized with amine ($-NH_2$) groups through nitration followed by

[a]*Shanghai Key Lab of Chemical Assessment and Sustainability, Department of Chemistry, Tongji University, Shanghai 200092, P. R. China. E-mail: bxiangbo@tongji.edu.cn; hongbogu2014@tongji.edu.cn*

[b]*Integrated Composites Lab (ICL), Department of Chemical & Biomolecular Engineering, University of Tennessee, Knoxville, Tennessee, 37966, USA. E-mail: zguo10@utk.edu*

† Electronic supplementary information (ESI) available. See DOI: 10.1039/c6ra09847a

reduction and reacted with carboxylic acid-terminated polyethylene glycol (PEG) chains, graphite nanosheets could serve as a promising carrier to deliver the anticancer drugs with improved water solubility.[24] Graphite oxide has been proved to have good weak acids adsorption capacity because of the presence of carboxylic and phenolic groups on the graphite surfaces.[25] Among these methods, surface oxidation is widely used in functionalization of graphite.[10,19] Even though there have been many emerging oxidation methods,[26–30] the degree of oxidation is too high so that graphite structure is seriously damaged. Hexavalent chromium (Cr(VI)) has a very strong oxidative ability in acidic solutions due to its high redox potential (1.33 V).[31] Though the Cr(VI) removal percentage and adsorption behaviors of functionalized graphite oxide materials from polluted water have been explored,[32,33] graphite functionalized by Cr(VI) was unfortunately rarely reported.

In the present work, the as-received graphite functionalized by Cr(VI) solutions using a simple ultrasonic method was investigated under different conditions. The effects of the pH value and initial Cr(VI) concentration on the graphite functionalization are explored systematically. After treatment with Cr(VI) solutions, the effects of surface functionality of graphite were studied by Raman spectroscopy, Fourier transform infrared spectroscopy (FT-IR), thermogravimetric analysis (TGA), and X-ray photoelectron spectroscopy (XPS). The electrical conductivity of the graphite functionalized by Cr(VI) was investigated and compared with the graphite oxide produced by modified Hummers method. The kinetics of the graphite in the Cr(VI) solutions with pH = 1.0 was also studied in details.

2. Experimental

2.1 Materials

Graphite (99.95% metals basis, average diameter: ≤1.3 μm) was provided by Aladdin Industrial Corporation, Shanghai. Acetone was supplied by Chinasun Specialty Products Co., Ltd, Jiangsu. Potassium dichromate ($K_2Cr_2O_7$, ≥99.8%), phosphorus pentoxide (P_2O_5, ≥98.0%), potassium persulfate ($K_2S_2O_8$, ≥99.5%), potassium permanganate ($KMnO_4$, ≥99.5%), sulfuric acid (H_2SO_4, 98 wt%), hydrochloric acid (HCl, 36.0–38.0 wt%), phosphoric acid (H_3PO_4, 85 wt%), hydrogen peroxide aqueous solution (PERDROGEN® 30% H_2O_2 (w/w)), 1,5-diphenylcarbazide (DPC) and ethanol were purchased from Sinopharm Chemical Reagent Co., Ltd, China. All the chemicals were used as-received without any further treatment.

2.2 Preparation of pre-oxidized graphite (pre-graphite)

In order to improve the hydrophilicity of graphite, the as-received graphite powders were first undergone a preoxidation process. Briefly, graphite powders (3.0 g), $K_2S_2O_8$ (4.0 g) and P_2O_5 (4.0 g) were weighed and mixed, then the mixture was slowly added into 12 mL concentrated H_2SO_4 (98.0, wt%), the mixture was heated in an oil bath at 80 °C and kept for 6 h. After cooling down to room temperature, deionized water was used to wash the products until pH was about 7. Then the preoxidized graphite was dried in air oven at 60 °C for 24 hours.

2.3 Functionalized graphite with Cr(VI) under different conditions

The $K_2Cr_2O_7$ stock solution (1.0 g L^{-1}) was prepared by dissolving $K_2Cr_2O_7$ (0.2829 g) into 100.0 mL deionized water. The Cr(VI) standard solution 400, 600, 800, 1000, 1100, 1200, 1600, 2000, 2500 and 4000 μg L^{-1} were prepared by diluting 40.0, 60.0, 80.0, 100.0, 110.0, 120.0, 160.0, 200.0, 250.0, and 400.0 μL potassium dichromate stock solution to 100.0 mL with deionized water, respectively. The DPC solution was prepared by dissolving 80.0 mg DPC in 20.0 mL acetone (prepared freshly for each use). The diluted H_3PO_4 (50% v/v) was prepared by diluting 50.0 mL concentrated phosphoric acid (85.0, wt%) to 100.0 mL with deionized water. The used H_2SO_4 (50% v/v) was prepared by diluting 50.0 mL concentrated H_2SO_4 (98.0, wt%) to 100.0 mL with deionized water.

2.4 Fabrication of graphite oxides by modified Hummer method

The dried pre-graphite powder was dispersed in 120.0 mL concentrated H_2SO_4 (98.0, wt%) in an ice-water bath, followed by gradual addition of 15.0 g $KMnO_4$. The magnetic stirring was continued during this process to remove the heat. The mixture was then magnetically stirred at 35 °C for 2 h. After that, the deionized water (250.0 mL) was added and magnetic stirring was continued for additional 15 min. Finally, the reaction was terminated by adding deionized water (700.0 mL) and H_2O_2 solution (30 wt%, 20 mL). After cooling down to room temperature, the solution was turned from blackish purple to bright yellow. The products were filtered and washed with 1 L HCl aqueous solution (1 : 9 v/v) to remove metal ions. The deionized water was used to centrifuge the products until pH was turned to neutral. The bright yellow product was placed in a freeze-dryer (FD-1A-50, Beijing Boyikang Laboratory Instruments Co., Ltd) and vacuum freeze-dried at −52 °C and vacuum pressure less than 30 Pa for 48 h.

2.5 Cr(VI) concentration determination

The final Cr(VI) concentration was determined by colorimetric method. The obtained standard fitting curve was $C = 1.2677 \times A$, where A is the absorbance obtained from the UV-vis spectrophotometer (UV756CRT, Shanghai Youke Instrument Co., Ltd.) test, C is the Cr(VI) concentration, from which the final Cr(VI) concentration of the solution was calculated.

The pH value effect on the graphite oxidation by Cr(VI) was investigated by selecting solutions with a pH value of 1.0, 2.0, 3.0, 5.0, 7.0, 9.0, and 11.0 at room temperature, respectively. The initial pH values of the Cr(VI) solutions were adjusted by 1.0 mol L^{-1} NaOH and 1.0 mol L^{-1} HCl with a pH meter (PHS-3E, Shanghai INESA Scientific Instrument Co., Ltd.), the pH = 1.0 Cr(VI) solution was adjusted by concentrated H_2SO_4 (98.0, wt%). The pre-graphite powders (20.0 mg) were ultrasonically dispersed in 20.0 mL solution with an initial Cr(VI) concentration of 1000.0 μg L^{-1} for 30 min by ultrasonic reactor (SK3200H, Shanghai Kudos Ultrasonic instrument Co., Ltd.). Then this solution was taken out and centrifuged (TDZ4B-WS, Shanghai

LuXiangYi Centrifuge Instrument Co., Ltd.) for Cr(VI) concentration determination. The supernatant (10.0 mL) was taken into a colorimetric tube, in which the diluted H_3PO_4 solution (0.10 mL), H_2SO_4 solution (0.10 mL) and DPC solution (0.40 mL) were added. After incubated at room temperature for 10 min for color development, an appropriate portion of the above solution was transferred to a one cm cuvette for UV-vis test.

The effect of initial Cr(VI) concentration on the Cr(VI) oxidation to the graphite was investigated by pre-graphite (20.0 mg) to treat pH = 1.0 Cr(VI) solutions (20.0 mL) with initial Cr(VI) concentration varying from 400.0 to 2000.0 μg L^{-1} for 30 min.

In order to evaluate the degree of structural change of the pre-graphite after treated with Cr(VI) solution, the pre-graphite (20.0 mg) was treated with pH = 1.0 Cr(VI) solutions (20.0 mL) with initial Cr(VI) concentration of 2500.0 and 4000.0 μg L^{-1} for 30 min, respectively.

For kinetic study, the pre-graphite powders (20.0 mg) were carried out to treat 20.0 mL pH = 1.0 solution with an initial Cr(VI) concentration of 1000.0 μg L^{-1} over different treatment periods from 5 to 30 min.

The Cr(VI) removal percentage (R%) was obtained by eqn (1):

$$R\% = \frac{C_0 - C_e}{C_0} \times 100\% \quad (1)$$

where C_0 (mg L^{-1}) is the initial Cr(VI) concentration, and C_e is the final Cr(VI) concentration of the solution after treatment. All the Cr(VI) removal tests were carried out at room temperature.

2.6 Characterizations

The Raman spectra (Invia, Renishaw) was used with 785 nm laser excitation at a 1.5 cm^{-1} resolution at room temperature. The thermogravimetric analysis (TGA, STA409 PC, Netzsch) was conducted at a heating rate of 20 °C min^{-1} and an air flow rate of 30 mL min^{-1} from 30 to 1000 °C. The Fourier transform infrared spectroscopy (FT-IR, Thermo Nicolet NEXUS, Thermo Scientific) was used to obtain the spectra in the range of 500 to 4000 cm^{-1} with a resolution of 4 cm^{-1}. X-ray Photoelectron Spectroscopy (XPS) analysis was carried out on a Kratos AXIS Ultra DLD instrument using monochromatic Al Kα radiation. The C 1s peaks were deconvoluted into the components consisting of a Gaussian line shape Lorentzian function (Gaussian = 80%, Lorentzian = 20%) on a Shirley background. The electrical conductivity was measured with a standard four-point method at room temperature using a KDY-1 electric and sheet resistance meter (Guangzhou, China).

3. Results and discussion

3.1 Effect of Cr(VI) concentration on the functionalization of graphite

The solution pH is one of the most important variables affecting the Cr(VI) oxidation stability. In the aqueous solution, the most important Cr(VI) ion forms in solution are chromate (CrO_4^{2-}), dichromate ($Cr_2O_7^{2-}$) and hydrogen chromate ($HCrO_4^-$) and these ion forms are related to the solution pH and total chromate concentration.[34] In the aqueous solution, dichromate ions ($Cr_2O_7^{2-}$) are in equilibrium with chromate ions (CrO_4^{2-}), eqn (2):[35]

$$Cr_2O_7^{2-} + H_2O \leftrightarrow 2CrO_4^{2-} + 2H^+ \quad (2)$$

This is a dynamic equilibrium and sensitive to the solution pH. When the solution is acidic, the equilibrium shifts to the left towards dichromate ions, which will spontaneously turn to $Cr_2O_7^{2-}$ as the dominating ions. However, as the solution is basic, the equilibrium shifts to the right and CrO_4^{2-} is the only chromate in the solution.[31] The Cr(VI) removal efficiency in different pH solutions (20.0 mL) with an initial Cr(VI) concentration of 1000 μg L^{-1} after 30 min treatment with 20.0 mg pre-graphite is shown in Fig. 1a. The Cr(VI) removal percentage by the pre-graphite is observed to be strongly depended on the pH values of the solution, which is found to be decreased with increasing the pH value from pH = 1.0 to 11.0. The Cr(VI) has been removed completely in the pH = 1.0 and the Cr(VI) removal percentage is sharply decreased with increasing the pH of solution. The Cr(VI) removal percentage for pH = 7.0, 9.0, and 11.0 is 21.4, 17.2, 15.3%, respectively. These results indicate that the Cr(VI) removal percentage by the pre-graphite is insufficient as the pH of solution is higher than 3, especially in the base solution.

Fig. 1b shows the Cr(VI) removal percentage for 20.0 mg pre-graphite with different initial Cr(VI) concentrations at pH of 1.0 over a treatment period of 30 min. The Cr(VI) is observed to be completely removed from the solutions with the initial Cr(VI) concentration ranging from 400.0 to 800.0 μg L^{-1}. After further increasing the initial Cr(VI) concentration, the Cr(VI) removal percentage of pre-graphite decreases to 68.4% for a solution with an initial Cr(VI) concentration of 1200 μg L^{-1}, only around 43.8% of the Cr(VI) is removed as the initial Cr(VI) concentration is increased to 2000 μg L^{-1}. Due to the large specific surface area of graphite, it has many active sites to react with Cr(VI). As the gradual saturation of these active sites occurs at high Cr(VI) concentrations, the graphite cannot accommodate excess Cr(VI), leading to a decreased Cr(VI) removal percentage.[36] These results are also observed for the Cr(VI) adsorbed by the magnetic amine-functionalized polyacrylic acid-nanomagnetite.[37]

The Raman spectrum is a prominent tool to characterize crystalline structure of carbon materials, especially for those possessing conjugated C=C bonds. With a strong response to specific electronic property,[38,39] it can provide valuable information about defects, stacking of the graphene layers and crystallite size to the hexagonal axis. These structure characters of carbon materials are normally not detectable by other analytical tools.[31] To better understand the degree of surface structural change of graphite in the course of interaction with Cr(VI), the graphite treated with pH = 1.0, 2.0, 7.0 and 11.0 Cr(VI) solution (1000 μg L^{-1}) for 30 min was analyzed by Raman spectrum, respectively, Fig. 2a. In Raman spectrum of the as-received graphite, two prominent bands at around 1345 and 1575 cm^{-1} are observed, corresponding to the local defects or disordered atomic arrangement of sp^3-carbon (D-band) and the plane vibration of the sp^2-carbon in the two dimensional lattice (G-band), respectively.[40] Normally, the higher the intensity of

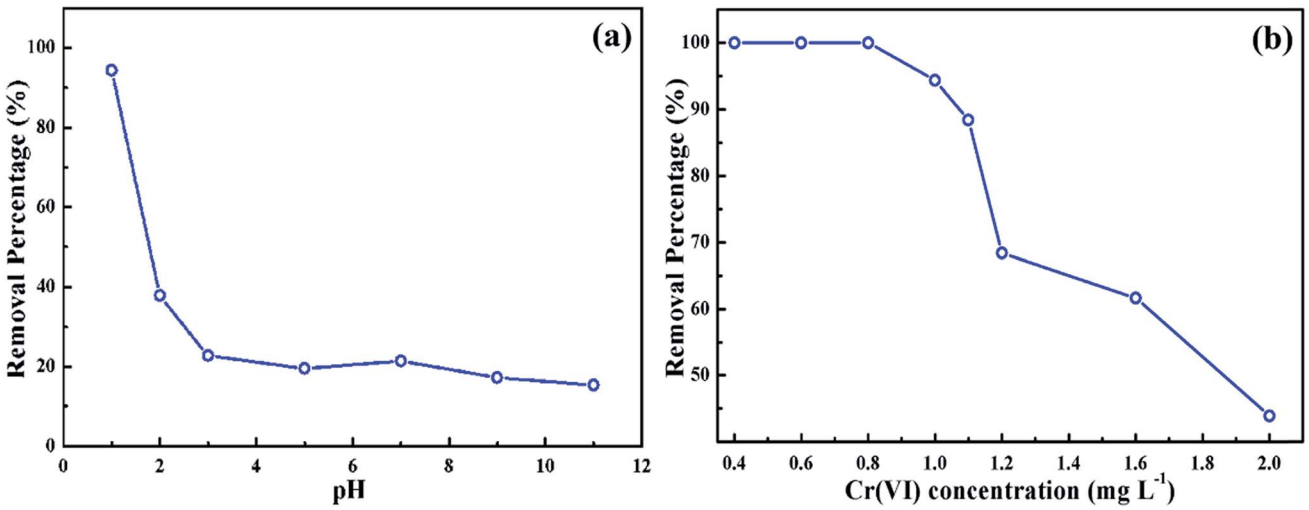

Fig. 1 Removal percentage of 20.0 mg pre-graphite for 20.0 mL Cr(VI) solutions with different (a) pH values after 30 min ultrasonic treatment at initial Cr(VI) concentrations of 1000 μg L^{-1} at room temperature; (b) initial Cr(VI) concentrations after 30 min ultrasonic treatment at pH of 1.0 at room temperature.

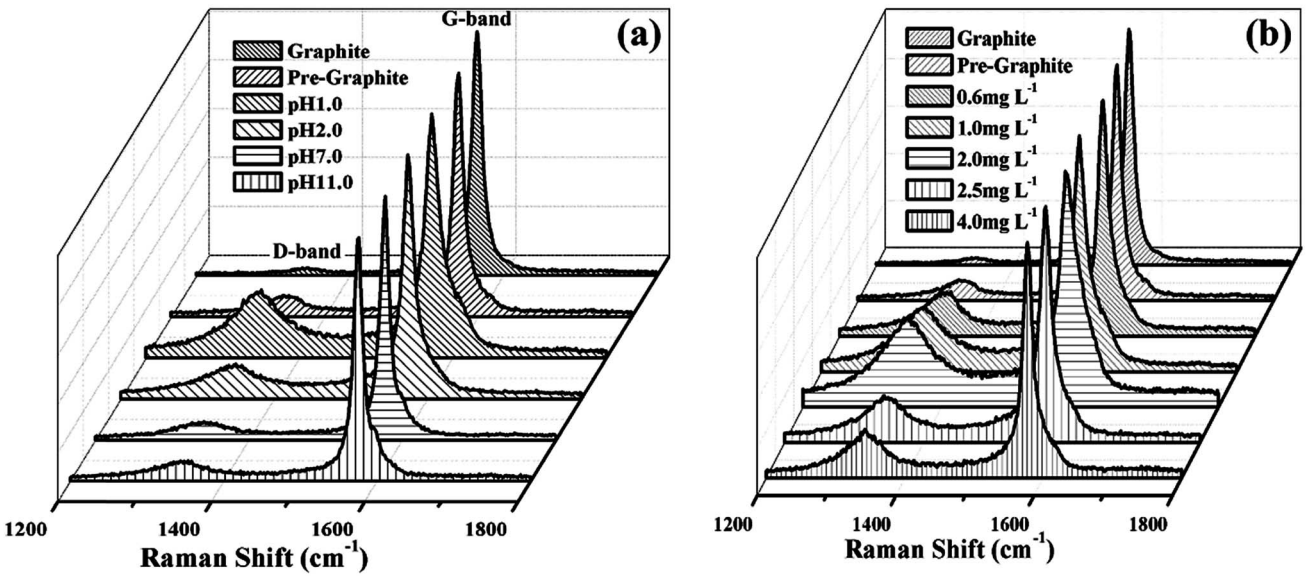

Fig. 2 Raman spectra of (a) as-received graphite, pre-graphite and pre-graphite samples treated with 1000 μg L^{-1} Cr(VI) solution with different pH values ranging from 1.0 to 11.0 after treated with 30 min; and (b) pre-graphite samples treated with pH = 1.0 Cr(VI) solution with different initial Cr(VI) concentrations ranging from 600 to 4000 μg L^{-1} Cr(VI) solution after treated with 30 min.

D-band, the more the oxygen species are formed on the graphite, and the more the oxygen-related functional groups are introduced on the graphite surface.[41] For the pre-graphite, there is no clear D-band intensity increased in the Raman spectrum, indicating no obvious change for the structure of graphite after pre-oxidation process. However, for the pre-graphite samples treated with 1000 μg L^{-1} pH = 1.0 Cr(VI) solution, the intensity of D-band is found to be continuously increased, and the intensity of G-band is slightly suppressed. For the pre-graphite treated with pH = 2.0 Cr(VI) solution, the intensity of D-band is also increased, but a little bit lower than that of in the Cr(VI) solution with pH of 1.0. There is no clear D-band intensity increased with further increasing the pH of solution. These results indicate that the graphite is functionalized with the oxygen related functional groups after treated with 1000 μg L^{-1} pH = 1.0 Cr(VI) solution. The graphite treated with different Cr(VI) concentrations in the pH = 1.0 solutions are also analyzed by Raman spectrum, Fig. 2b. In Fig. 2b, the intensity of D-band is observed to increase with increasing the Cr(VI) concentration. However, as Cr(VI) concentration is higher than 2 mg L^{-1}, the D-band decreases with increasing the Cr(VI) concentration. This may be due to the fact that Cr(VI) and graphite form complex compounds with Cr(VI) concentration higher than 2 mg L^{-1}. This phenomenon was also observed in the Cr(VI) functionalized multi-walled carbon nanotubes (MWNTs).[31]

To further understand the degree of surface structural change of the graphite after treated with different pH values of Cr(VI) solutions, the FT-IR spectra of graphite treated with Cr(VI) solutions in different conditions are obtained, Fig. 3A. In the FT-IR spectrum of pre-graphite and pre-graphite treated with different pH values of Cr(VI) solutions, the broad band at around

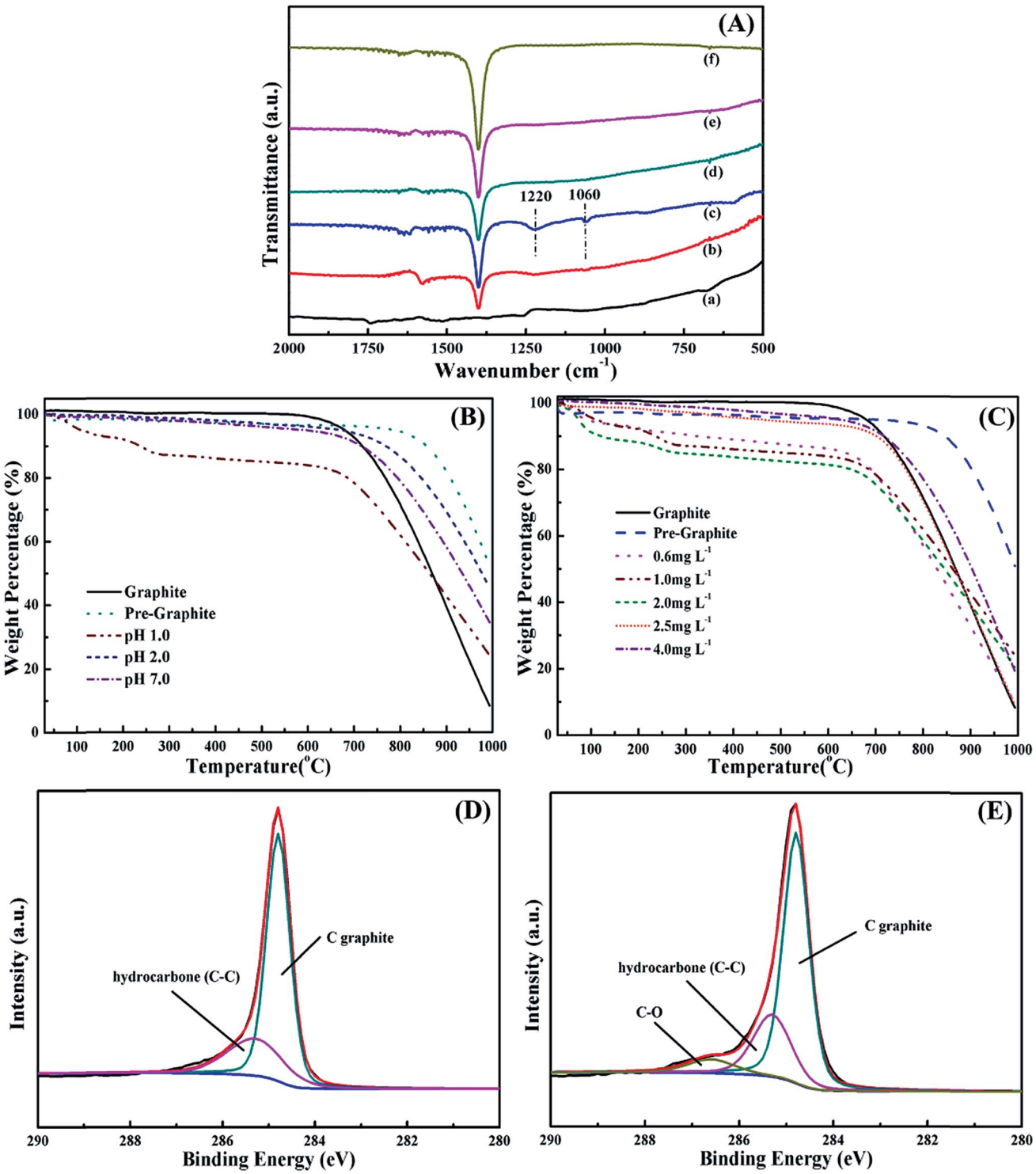

Fig. 3 (A) FT-IR spectra of (a) graphite, (b) pre-graphite and pre-graphite samples treated with 1000 μg L^{-1} Cr(VI) solutions with a pH value of (c) 1.0, (d) 3.0, (e) 7.0, and (f) 9.0 for the treatment time of 30 min; TGA curves of (B) graphite, pre-graphite and pre-graphite treated with 1000 μg L^{-1} Cr(VI) solution with different pH values ranging from 1.0 to 7.0 for the treatment time of 30 min, and (C) graphite, pre-graphite and pre-graphite treated with pH = 1.0 Cr(VI) solution with different initial Cr(VI) concentrations ranging from 600 to 4000 μg L^{-1} Cr(VI) solution after treated with 30 min; deconvoluted C 1s high resolution XPS spectra of (D) graphite, and (E) pre-graphite treated with 1000 μg L^{-1} Cr(VI) with pH = 1.0 solution for 30 min.

1400 cm^{-1} is assigned to the C–H in-plane band, confirming the presence of C–H in the pre-graphite.[42] In the FT-IR spectrum of pre-graphite sample treated with pH = 1.0 Cr(VI) solution, Fig. 3A–C, the broad band at around 1060–1220 cm^{-1} corresponds to the C–O–C stretching vibration, which is obvious in the FT-IR spectra of other samples. This indicates that graphite was functionalized with ether group after treatment with 1000 μg L^{-1} pH = 1.0 Cr(VI) solution. Cr(VI) is known as a very strong oxidant due to its high redox potential, eqn (3), especially in pH < 2.0 acidic solutions:[43,44]

$$Cr_2O_7^{2-} + 14H^+ + 6e^- \leftrightarrow 2Cr^{3+} + 7H_2O,\ E_0 = 1.33\ V \quad (3)$$

This indicates that a redox reaction occurred in the pH = 1.0 solution, demonstrating that the graphite has been oxidized by Cr(VI) after treatment with pH = 1.0 Cr(VI) solution and the C–O–C is formed on the surface of graphite. Similar result was also observed in the Cr(VI) treated MWNTs.[31] However, in Fig. 3A, the pre-graphite samples after treated with pH = 3.0, 7.0 and 9.0 Cr(VI) solutions are almost the same as that of the pre-graphite, indicating no functional groups formed in the graphite samples after treated with pH > 2.0 Cr(VI) solutions, which is in agreement with the Raman spectrum.

TGA is a complementary technique utilized to investigate the thermal stability of materials.[45] To further explore the interactions between graphite and Cr(VI) in the solutions with different pH values, the graphite samples treated with different pH solutions were studied with TGA analysis. In the TGA curves, Fig. 3B, the graphite exhibits only one-stage weight loss at 600 °C due to the thermal degradation of the hexagonal structure of graphite in the air. However, the weight loss of pre-graphite is occurred at 800 °C, higher than that of the graphite, meaning that the pre-treatment process can enhance the thermal stability of graphite. Two-stage weight losses are observed in the pre-graphite sample treated with pH = 1.0 Cr(VI) solution. The first stage from 200 to 250 °C is attributed to the degradation of the C–O–C groups,[31] which is in good agreement with the results of FT-IR analysis. After that, a plateau during the temperature range from 250 to 630 °C is observed. The second weight loss of sample from 630 to 1000 °C is also from the thermal degradation of hexagonal structure of graphite. For other samples, similar thermal degradation processes are observed. The degradation temperature is 710 and 660 °C for the pre-graphite treated with pH = 2.0 and 7.0 Cr(VI) solutions, respectively, which are lower than that of the pre-graphite. These results suggest that the pre-graphite treated with Cr(VI) solution has a significant impact on the thermal stability of pre-graphite. It's concluded that when pH of solution is lower than 2.0, the Cr(VI) solution has a significant effect on the thermal stability of the pre-graphite, but the effect is not obvious as pH is >2.0.

The graphite samples treated with pH = 1.0 solutions different Cr(VI) concentrations are also studied with TGA analysis and the results are shown in Fig. 3C. Interestingly, it's observed that when Cr(VI) concentration is <2.0 mg L^{-1}, significant degradation from 200 to 250 °C is observed, indicating that the graphite is functionalized with the C–O–C groups after treated with Cr(VI) solution as aforementioned and the content of C–O–C groups is increased with increasing the Cr(VI) concentrations. However, after the Cr(VI) concentration is higher than 2.0 mg L^{-1}, the TGA curve of samples starts to show different decomposition profiles from that of samples treated with Cr(VI) concentration <2.0 mg L^{-1}. This phenomenon is similarly found in the Raman test, Fig. 2b.

XPS is a very useful analysis tool to investigate the atomic composition and chemical environment of the outermost few nanometers layer of a surface, which can accurately determine the surface coverage.[46] In order to confirm that the graphite is

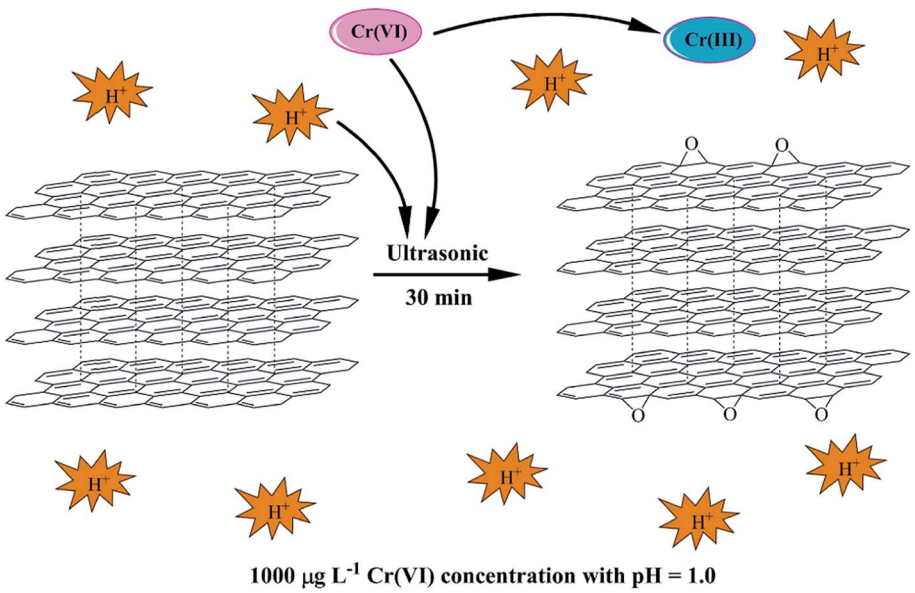

Scheme 1 The proposed formation mechanism of functionalized graphite process.

functionalized by the Cr(VI) solution, the electronic structure of the graphite is also analyzed by XPS spectra. Fig. 3D and E are the C 1s XPS spectra of the graphite and the pre-graphite treated with pH = 1.0 Cr(VI) solution. The C 1s peak of the graphite can be deconvoluted into two components situated at the binding energy of 284.8 and 285.3 eV, which can be assigned to C=C and hydrocarbone C–C, respectively.[47,48] However, for the pre-graphite treated with pH = 1.0 Cr(VI) solution, the C 1s peak can be smoothly fixed into three peaks at 284.8, 285.3, and 286.6 eV, respectively. The new peak at 286.6 eV is attributed to the C–O groups,[49] indicating that the C–O groups exist on the graphite surface after treated with Cr(VI) solution. This result is consistent with the observation of FT-IR analysis and TGA curves. Based on all the aforementioned analyses, the proposed formation process of functionalized graphite is presented in Scheme 1. Under the ultrasonic process, the surface of the pre-graphite is fully exposed in the solution. In acid conditions, the graphite is functionalized with the ether group after treated with Cr(VI) solution, and the Cr(VI) is reduced to Cr(III).

3.2 Electrical conductivity analysis

The electrical conductivity of graphite, pre-graphite and pre-graphite treated with pH = 1.0 Cr(VI) solution is measured and listed in Fig. 4a. The volume resistivity of graphite, pre-graphite and pre-graphite treated with pH = 1.0 Cr(VI) solution is 1.7×10^{-3}, 1.9×10^{-3} and 2.2×10^{-3} Ω cm, respectively. It is worth noting that the volume resistivity of graphite barely changes after treated with Cr(VI) solution, demonstrating that the graphite structure is not significantly damaged compared with the as-received graphite. The volume resistivity of graphite oxide produced by modified Hummers method procedure is also measured for comparison. However, its volume resistivity is too high, which is beyond the measuring range of the instrument (>10^4 Ω cm). Normally, the oxidation degree by the Hummers process is too strong and the graphite structure is seriously damaged, resulting in the highly decreased conductivity of graphite. Therefore, even the graphite oxide prepared by Hummers method is commonly used for fabricating the graphite–polymer nanocomposites, the high electrical conductivity is hard to achieve. The Cr(VI) oxidation is a simple and effective method to prepare the graphite oxide, which can maintain the excellent electrical conductivity of graphite.

3.3 Cr(VI) oxidation kinetics

The kinetics of pre-graphite oxidation in the Cr(VI) solution is one of the important parameters to describe the pre-graphite oxidation rate. Hence, in the present study, the kinetics of the pre-graphite oxidation in the pH = 1.0 Cr(VI) solution (1000 μg L^{-1}) is studied and the Cr(VI) concentration change during the treatment period (5, 10, 15, 20 and 30 min) is shown in Fig. S1.† The Cr(VI) concentration in the solution during a 30 min treatment period decreases from 1000.0 to 57.433 μg L^{-1}.

An appropriate kinetic model is required to quantify the amount changes of Cr(VI) concentration with time. The pseudo-first-order behavior has been reported for the Cr(VI) reduction by polyaniline film,[50] polyaniline–magnetite (Fe_3O_4) nanocomposites[35] and MWNTs.[31] Therefore, the pseudo-first-order kinetics is introduced to describe the pre-graphite oxidation behavior. The reduction of Cr(VI) with graphite is described by eqn (4):

$$HCrO_4^- (aq) + H^+ + \text{pre-graphite (s)} \rightarrow Cr^{3+} (aq) + \text{pre-graphite–O (s)} + H_2O \quad (4)$$

where pre-graphite–O refers to the oxidized pre-graphite after treated with Cr(VI). From eqn (4), the rate of this reaction is observed to depend on three different species: $HCrO_4^-$, H^+ and graphite. Accordingly, the reaction rate may be expressed by eqn (5):

$$v = \frac{d[Cr(VI)]}{dt} = -k[HCrO_4^-]^m[\text{pre-graphite}]^n[H^+]^p \quad (5)$$

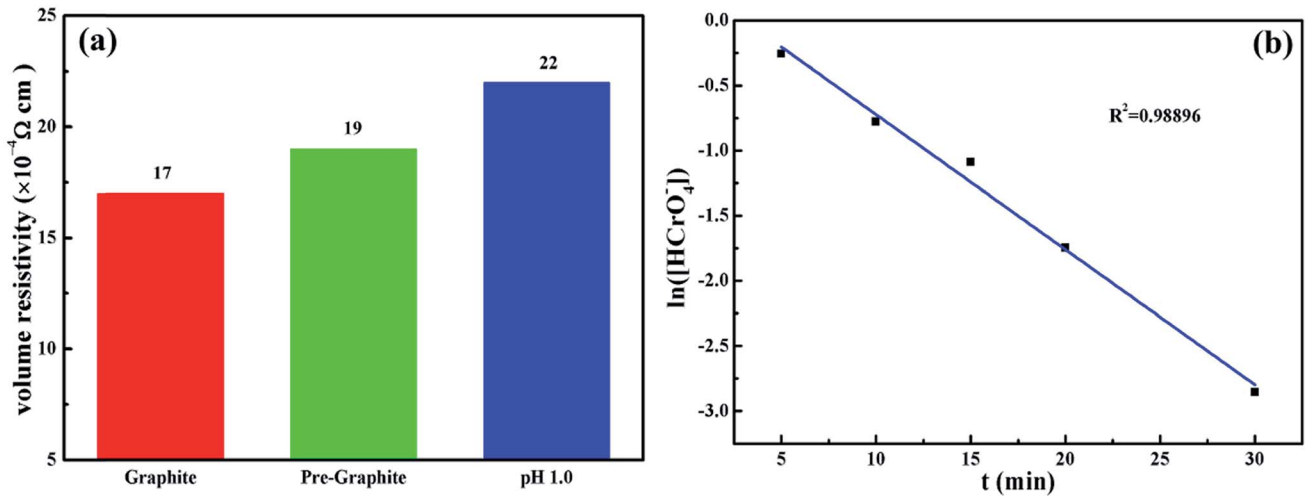

Fig. 4 (a) Volume resistivity of graphite, pre-graphite and pre-graphite after treated with 1000 μg L^{-1} Cr(VI) with pH = 1.0 solution for 30 min; and (b) kinetic plot of ln([$HCrO_4^-$]) *vs.* *t* for 20.0 mg pre-graphite sample after treatment with 20.0 mL 1000 μg L^{-1} Cr(VI) solution (pH = 1.0) under different treatment times at room temperature.

where k is the rate constant, the exponents (m, n and p) are called reaction orders, which depend on the reaction mechanism; and $[HCrO_4^-]$, [pre-graphite] and $[H^+]$ are the concentration of $HCrO_4^-$, graphite, H^+ at any time, respectively. However, since H^+ serves as catalyst in this reaction,[35] and pre-graphite is solid and its concentration are much higher than $[HCrO_4^-]$, which means that the $[HCrO_4^-]$ is the dominating species to control the reaction rate. Therefore, eqn (5) can be rewritten as eqn (6):

$$v = \frac{d[Cr(VI)]}{dt} = k'\left[HCrO_4^-\right]^1 \quad (6)$$

where k' stands for a pseudo-first-order rate constant. The obtained corresponding kinetic plot is shown in Fig. 4b. The observed linear relation between $\ln([HCrO_4^-])$ and t with a fitting correlation coefficient R^2 of 0.98896 indicates a pseudo-fist-order reaction between Cr(VI) and graphite. The calculated rate constant k' calculated from the slope is 0.1038 min^{-1}. The calculated rate constant k' calculated from the slope is 0.1038 min^{-1}, which is higher than that of polyaniline film (0.0024 min^{-1}),[50] MWNTs (0.05786 min^{-1}),[31] and lower than that of polyaniline–Fe_3O_4 nanocomposites (0.185 min^{-1}).[35]

4. Conclusions

Graphite oxide has been successfully prepared by Cr(VI) solutions. Before functionalized by the Cr(VI) solutions, the graphite powders were first undergone a preoxidation process to improve the hydrophilicity of the graphite. The Raman spectroscopy, FT-IR, TGA and XPS characterizations indicate that the pre-graphite has been functionalized with C–O–C groups after treated with pH = 1.0 Cr(VI) solution (1000 μg L^{-1}) with a treatment period of 30 min. However, as the solution pH higher than 2.0 or the Cr(VI) concentrations higher than 2.0 mg L^{-1}, there are no obvious functional groups on the pre-graphite surface. The electrical conductivity measurements indicate that the pre-graphite after treated with pH = 1.0 Cr(VI) solution (1000 μg L^{-1}) with 30 min still maintains excellent conductivity of graphite, the volume resistivity still keeps the same order of magnitude as the graphite. The kinetics indicates that in the process of functionalization at pH = 1.0 of Cr(VI) solution, the redox kinetics dominates the Cr(VI) removal process and exhibits a pseudo-first-order behavior with respect to Cr(VI) concentration. The calculated pseudo-first-order rate constant is 0.1038 min^{-1}. This exploration provides a potential application for preparing the multifunctional polymer nanocomposites, such as graphite reinforced epoxy nanocomposites with excellent electrical conductivity.[51]

References

1 C.-G. Lee, Y.-J. Hwang, Y.-M. Choi, J.-K. Lee, C. Choi and J.-M. Oh, *Int. J. Precis. Eng. Manuf.*, 2009, **10**, 85–90.
2 B. Gupta, K. Panda, N. Kumar, A. A. Melvin, S. Dash and A. K. Tyagi, *RSC Adv.*, 2015, **5**, 53766–53775.
3 F. Ding, W. Xu, D. Choi, W. Wang, X. Li, M. H. Engelhard, X. Chen, Z. Yang and J.-G. Zhang, *J. Mater. Chem.*, 2012, **22**, 12745–12751.
4 S. Luo and T. Liu, *Adv Mater.*, 2013, **25**, 5650–5657.
5 H. Wang, H. Yi, C. Zhu, X. Wang and H. J. Fan, *Nano Energy*, 2015, **13**, 658–669.
6 H. Yi, H. Wang, Y. Jing, T. Peng and X. Wang, *J. Power Sources*, 2015, **285**, 281–290.
7 P. Tang, L. Han and L. Zhang, *ACS Appl. Mater. Interfaces*, 2014, **6**, 10506–10515.
8 X. Xia, D. Chao, Z. Fan, C. Guan, X. Cao, H. Zhang and H. J. Fan, *Nano Lett.*, 2014, **14**, 1651–1658.
9 J. Gu, X. Yang, Z. Lv, N. Li, C. Liang and Q. Zhang, *Int. J. Heat Mass Transfer*, 2016, **92**, 15–22.
10 J. Gu, N. Li, L. Tian, Z. Lv and Q. Zhang, *RSC Adv.*, 2015, **5**, 36334–36339.
11 J. Gu, J. Du, J. Dang, W. Geng, S. Hu and Q. Zhang, *RSC Adv.*, 2014, **4**, 22101–22105.
12 H. Gu, X. Zhang, H. Wei, Y. Huang, S. Wei and Z. Guo, *Chem. Soc. Rev.*, 2013, **42**, 5907–5943.
13 A. Boden, B. Boerner, P. Kusch, I. Firkowska and S. Reich, *Nano Lett.*, 2014, **14**, 3640–3644.
14 I. Firkowska, A. Boden, B. Boerner and S. Reich, *Nano Lett.*, 2015, **15**, 4745–4751.
15 A. Pai, S. S. Sharma, R. E. D'Silva and R. G. Nikhil, *Tribol. Int.*, 2015, **92**, 462–471.
16 Y. Lee, M. R. Jo, K. Song, K. M. Nam, J. T. Park and Y. M. Kang, *ACS Appl. Mater. Interfaces*, 2012, **4**, 3459–3464.
17 A. L. Higginbotham, J. R. Lomeda, A. B. Morgan and J. M. Tour, *ACS Appl. Mater. Interfaces*, 2009, **1**, 2256–2261.
18 J. Gao, M. Hu, Y. Dong and R. K. Y. Li, *ACS Appl. Mater. Interfaces*, 2013, **5**, 7758–7764.
19 M. R. Karim, Y. Ikeda, T. Ide, S. Sugimoto, K. Toda, Y. Kitamura, T. Ihara, T. Matsui, T. Taniguchi, M. Koinuma, Y. Matsumoto and S. Hayami, *New J. Chem.*, 2014, **38**, 2120.
20 J. Chattopadhyay, A. Mukherjee, S. Chakraborty, J. Kang, P. J. Loos, K. F. Kelly, H. K. Schmidt and W. E. Billups, *Carbon*, 2009, **47**, 2945–2949.
21 A. Mukherjee, J. Kang, O. Kuznetsov, Y. Sun, R. Thaner, A. S. Bratt, J. R. Lomeda, K. F. Kelly and W. E. Billups, *Chem. Mater.*, 2011, **23**, 9–13.
22 B. Standley, A. Mendez, E. Schmidgall and M. Bockrath, *Nano Lett.*, 2012, **12**, 1165–1169.
23 A. Abdolmaleki, S. Mallakpour and S. Borandeh, *RSC Adv.*, 2014, **4**, 60052–60057.
24 A. Chakravarty, K. Bhowmik, G. De and A. Mukherjee, *New J. Chem.*, 2015, **39**, 2451–2458.
25 A. M. Moustafa, K. N. McPhedran, J. Moreira and M. Gamal El-Din, *Environ. Sci. Technol.*, 2014, **48**, 14472–14480.
26 F. Perreault, A. Fonseca de Faria and M. Elimelech, *Chem. Soc. Rev.*, 2015, **44**, 5861–5896.
27 J. Zhu, M. Chen, H. Qu, X. Zhang, H. Wei, Z. Luo, H. A. Colorado, S. Wei and Z. Guo, *Polymer*, 2012, **53**, 5953–5964.
28 G. Zhao, X. Ren, X. Gao, X. Tan, J. Li, C. Chen, Y. Huang and X. Wang, *Dalton Trans.*, 2011, **40**, 10945–10952.

29 J. R. Lomeda, C. D. Doyle, D. V. Kosynkin, W.-F. Hwang and J. M. Tour, *J. Am. Chem. Soc.*, 2008, **130**, 16201–16206.
30 H.-K. Jeong, Y. P. Lee, R. J. W. E. Lahaye, M.-H. Park, K. H. An, I. J. Kim, C.-W. Yang, C. Y. Park, R. S. Ruoff and Y. H. Lee, *J. Am. Chem. Soc.*, 2008, **130**, 1362–1366.
31 H. Gu, S. B. Rapole, Y. Huang, D. Cao, Z. Luo, S. Wei and Z. Guo, *J. Mater. Chem. A*, 2013, **1**, 2011–2021.
32 G. Gollavelli, C.-C. Chang and Y.-C. Ling, *ACS Sustainable Chem. Eng.*, 2013, **1**, 462–472.
33 Y. Yang, M. H. Diao, M. M. Gao, X. F. Sun, X. W. Liu, G. H. Zhang, Z. Qi and S. G. Wang, *Electrochim. Acta*, 2014, **132**, 496–503.
34 J. Zhu, S. Wei, H. Gu, S. B. Rapole, Q. Wang, Z. Luo, N. Haldolaarachchige, D. P. Young and Z. Guo, *Environ. Sci. Technol.*, 2012, **46**, 977–985.
35 H. Gu, S. B. Rapole, J. Sharma, Y. Huang, D. Cao, H. A. Colorado, Z. Luo, N. Haldolaarachchige, D. P. Young, B. Walters, S. Wei and Z. Guo, *RSC Adv.*, 2012, **2**, 11007–11018.
36 J. Zhu, H. Gu, J. Guo, M. Chen, H. Wei, Z. Luo, H. A. Colorado, N. Yerra, D. Ding, T. C. Ho, N. Haldolaarachchige, J. Hopper, D. P. Young, Z. Guo and S. Wei, *J. Mater. Chem. A*, 2014, **2**, 2256–2265.
37 F. Gao, H. Gu, H. Wang, X. Wang and B. Xiang, *RSC Adv.*, 2015, **5**, 60208–60219.
38 H. Gu, J. Guo, Q. He, Y. Jiang, Y. Huang, N. Haldolaarachige, Z. Luo, D. P. Young, S. Wei and Z. Guo, *Nanoscale*, 2014, **6**, 181–189.
39 Y. Wang, Q. He, H. Qu, X. Zhang, J. Guo, J. Zhu, G. Zhao, H. A. Colorado, J. Yu, L. Sun, S. Bhana, M. A. Khan, X. Huang, D. P. Young, H. Wang, X. Wang, S. Wei and Z. Guo, *J. Mater. Chem. C*, 2014, **2**, 9478–9488.
40 L. Li, C. Zeng, L. Ai and J. Jiang, *J. Alloys Compd.*, 2015, **639**, 470–477.
41 Y. C. Jung, H. H. Kim, Y. A. Kim, J. H. Kim, J. W. Cho, M. Endo and M. S. Dresselhaus, *Macromolecules*, 2010, **43**, 6106–6112.
42 Y. Li, F. Yu, W. He and W. Yang, *RSC Adv.*, 2015, **5**, 2550–2561.
43 L. K. Cabatingan, R. C. Agapay, J. L. Rakels, M. Ottens and L. A. van der Wielen, *Ind. Eng. Chem. Res.*, 2001, **40**, 2302–2309.
44 I. M. Dittert, H. de Lima Brandão, F. Pina, E. A. da Silva, S. M. G. U. de Souza, A. A. U. de Souza, C. M. Botelho, R. A. Boaventura and V. J. Vilar, *Chem. Eng. J.*, 2014, **237**, 443–454.
45 C. Zeng, S. Lu, X. Xiao, J. Gao, L. Pan, Z. He and J. Yu, *Polym. Bull.*, 2014, **72**, 453–472.
46 E. Vanea and V. Simon, *Appl. Surf. Sci.*, 2011, **257**, 2346–2352.
47 C. Sharan, P. Khandelwal and P. Poddar, *RSC Adv.*, 2015, **5**, 91785–91794.
48 N. Moncoffre, G. Hollinger, H. Jaffrezic, G. Marest and J. Tousset, *Nucl. Instrum. Methods Phys. Res., Sect. B*, 1985, **7–8**, 177–183.
49 M. Bou, J. M. Martin, T. Le Mogne and L. Vovelle, *Appl. Surf. Sci.*, 1991, **47**, 149–161.
50 S. T. Farrell and C. B. Breslin, *Environ. Sci. Technol.*, 2004, **38**, 4671–4676.
51 X. Zhang, O. Alloul, Q. He, J. Zhu, M. J. Verde, Y. Li, S. Wei and Z. Guo, *Polymer*, 2013, **54**, 3594–3604.

